



Automatic Optimization of an *in Silico* Model of Human iPSC Derived Cardiomyocytes Recapitulating Calcium Handling Abnormalities

Michelangelo Paci^{1*}, Risto-Pekka Pölonen², Dario Cori³, Kirsi Penttinen²,
Katriina Aalto-Setälä^{2,4}, Stefano Severi^{3†} and Jari Hyttinen^{1†}

¹ Faculty of Biomedical Sciences and Engineering, BioMediTech Institute, Tampere University of Technology, Tampere, Finland, ² Faculty of Medicine and Life Sciences, BioMediTech Institute, University of Tampere, Tampere, Finland,

³ Department of Electrical, Electronic and Information Engineering "Guglielmo Marconi", University of Bologna, Cesena, Italy,

⁴ Heart Hospital, Tampere University Hospital, Tampere, Finland

OPEN ACCESS

Edited by:

Jichao Zhao,

University of Auckland, New Zealand

Reviewed by:

Jieyun Bai,

University of Auckland, New Zealand

Michelle M. Monasky,

Policlinico San Donato (IRCCS), Italy

Anuj Agarwal,

Signal Solutions LLC, Fairfax Virginia,

United States

*Correspondence:

Michelangelo Paci

michelangelo.paci@utu.fi

[†]These authors have contributed equally to this work.

Specialty section:

This article was submitted to Computational Physiology and Medicine,

a section of the journal Frontiers in Physiology

Received: 16 March 2018

Accepted: 22 May 2018

Published: 26 June 2018

Citation:

Paci M, Pölonen R-P, Cori D, Penttinen K, Aalto-Setälä K, Severi S and Hyttinen J (2018) Automatic Optimization of an *in Silico* Model of Human iPSC Derived Cardiomyocytes Recapitulating Calcium Handling Abnormalities. *Front. Physiol.* 9:709. doi: 10.3389/fphys.2018.00709

The growing importance of human induced pluripotent stem cell-derived cardiomyocytes (hiPSC-CMs), as patient-specific and disease-specific models for studying cellular cardiac electrophysiology or for preliminary cardiotoxicity tests, generated better understanding of hiPSC-CM biophysical mechanisms and great amount of action potential and calcium transient data. In this paper, we propose a new hiPSC-CM *in silico* model, with particular attention to Ca²⁺ handling. We used (i) the hiPSC-CM Paci2013 model as starting point, (ii) a new dataset of Ca²⁺ transient measurements to tune the parameters of the inward and outward Ca²⁺ fluxes of sarcoplasmic reticulum, and (iii) an automatic parameter optimization to fit action potentials and Ca²⁺ transients. The Paci2018 model simulates, together with the typical hiPSC-CM spontaneous action potentials, more refined Ca²⁺ transients and delayed afterdepolarizations-like abnormalities, which the old Paci2013 was not able to predict due to its mathematical formulation. The Paci2018 model was validated against (i) the same current blocking experiments used to validate the Paci2013 model, and (ii) recently published data about effects of different extracellular ionic concentrations. In conclusion, we present a new and more versatile *in silico* model, which will provide a platform for modeling the effects of drugs or mutations that affect Ca²⁺ handling in hiPSC-CMs.

Keywords: human induced pluripotent stem cell-derived cardiomyocyte, action potential, calcium transient, computer simulation, *in silico* modeling

INTRODUCTION

Human induced pluripotent stem cell-derived cardiomyocytes (hiPSC-CMs) are cardiac cells derived from stem cells, which have been produced by donor's differentiated cells by means of reprogramming (Takahashi et al., 2007). The role of hiPSC-CMs, has become more and more pervasive in basic electrophysiological studies as well as in applied research, such as pharmacological tests, since their discover in 2007. As an *in vitro* human model, hiPSC-CMs strongly impacted the study of biophysical mechanisms underlying cardiac electrophysiology at cellular level, both in control and diseased conditions. Especially hiPSC-CMs' patient- and

disease-specificity is fundamental to assess the effects of genetic mutations, such as Long QT (LQT) (Moretti et al., 2010; Lahti et al., 2012; Ma et al., 2013), catecholaminergic polymorphic ventricular tachycardia (CPVT) (Kujala et al., 2012) and hypertrophic cardiomyopathy (HCM) (Ojala et al., 2016), on the functionality of cardiomyocytes. Ever since the beginning of the Comprehensive *In vitro* Proarrhythmic Assay (CIPA) (<http://cipaproject.org/>) in 2013, hiPSC-CMs have had a dramatic impact on pharmacology, serving as a powerful *in vitro* model to test the *in silico* model predictions regarding cardiac safety or drug toxicity at cellular level.

During the last 10 years, many progresses were done in terms of efficiency of hiPSC-CM production and availability of commercial cell lines. This enabled also the hiPSC-CM electrophysiological and pharmacological evaluation by means of medium-throughput (Rajamohan et al., 2016) or even high-throughput systems (Entcheva and Bub, 2016; Klimas et al., 2016), where the use of voltage- and calcium-sensitive dyes has been combined with hiPSC-CM optogenetic stimulation. Together with the availability of these experimental data, new methods have been developed to process them (Björk et al., 2017; Ahola et al., 2018).

The importance of Ca^{2+} cycling to basic cardiac functionality, together with the growing availability of hiPSC-CM Ca^{2+} cycling data, makes Ca^{2+} transients, and biomarkers computed onto them, as interesting as action potential (AP) measurements. Ca^{2+} is fundamental in the heart excitation-contraction (EC) coupling, i.e., how the electrical and the mechanical properties of the heart are linked together and how the AP leads to the cardiomyocyte contraction. The elements involved in this phenomenon are the L-type Ca^{2+} channels, the sarcoplasmic reticulum (SR) and the sarcomeres, i.e., the contractile unit of the cardiomyocyte. During the AP upstroke, the L-type Ca^{2+} channels open and Ca^{2+} flows into the cardiomyocyte. This Ca^{2+} influx is sufficient to trigger the Ca^{2+} release from SR through the ryanodine-sensitive Ca^{2+} channels, which increases the cytosolic Ca^{2+} . Such amount of Ca^{2+} allows starting the crossbridge cycle, which is at the basis of the cardiomyocyte contraction and continues until Ca^{2+} is restored to its basal cytosolic concentration. This is mainly done by the SERCA-2 pump, which reabsorbs Ca^{2+} from the cytosol into the SR. Moreover, cytosolic Ca^{2+} is extruded into the extracellular space by the $\text{Na}^+/\text{Ca}^{2+}$ exchanger (I_{NaCa}) and by the sarcolemmal Ca^{2+} pump (I_{pCa}). All these mechanisms make the intracellular Ca^{2+} concentration change, thus producing Ca^{2+} transients associated to the APs (Walker and Spinale, 1999).

In 2013 we published the first *in silico* hiPSC-CMs model (Paci et al., 2013), based on our previous model of cardiomyocytes derived from human embryonic stem cells (Paci et al., 2012) and on the experimental data by Ma et al. (2011). This model has been widely used for computational studies, such as (i) the prediction of drug effects on cardiac electrophysiology (Paci et al., 2015; Lei et al., 2017), (ii) the model extension to multielectrode array simulations (Raphel et al., 2017), and (iii) the assessment of hiPSC-CM electrophysiological variability in control and mutant cells, by means of populations of *in silico* hiPSC-CMs (Paci et al., 2017). However, one of the Paci2013 model limitations resides in its formulations of the

Ca^{2+} handling system: especially the Ca^{2+} release from the sarcoplasmic reticulum (SR) is formulated with the functional but quite elementary Ca^{2+} release from the TenTusscher2004 model (ten Tusscher et al., 2004).

In this work, we propose an updated version of the Paci2013 hiPSC-CM ventricular-like model with a more flexible Ca^{2+} handling formulation. The Ca^{2+} transients produced by the model were calibrated on experimental Ca^{2+} imaging data recorded in our laboratory on hiPSC-CMs. Moreover, the fine tuning of the model parameters was performed by means of an automatic optimization technique (Fabbri et al., 2017), in order to reproduce realistic AP and Ca^{2+} transient shapes and to speed up the parameter tuning phase. Parameter optimization affected only the parameters representing the Ca^{2+} SR fluxes and a very limited set of parameters of membrane currents in order to be consistent with the voltage clamp experiment fitting done by Paci et al. (Paci et al., 2013). Finally, the resulting updated model was validated against ion current blocking data.

MATERIALS AND METHODS

New Ca^{2+} Handling System Formulation

The main limitation of the original Paci2013 model (Paci et al., 2013) and its following minor updates (Paci et al., 2015, 2017) is the simplified description of the Ca^{2+} release from SR, i.e., the release current I_{rel} . I_{rel} was formulated as in the TenTusscher2004 model (ten Tusscher et al., 2004) in the following way:

$$I_{\text{rel}} = K_{\text{rel}} \cdot \left(c_{\text{rel}} + \frac{a_{\text{rel}} \cdot \text{Ca}_{\text{SR}}^2}{b_{\text{rel}}^2 + \text{Ca}_{\text{SR}}^2} \right) \cdot d \cdot g$$

where K_{rel} , a_{rel} , b_{rel} , and c_{rel} are constants, Ca_{SR} is the Ca^{2+} concentration in the SR reticulum, d is the L-type Ca^{2+} current (I_{CaL}) voltage-dependent activation gate, and g is the I_{rel} specific inactivation gate. Therefore, I_{rel} is not activated by the cytosolic Ca^{2+} concentration Ca_i sensed by the Ryanodine-sensitive receptor located on the SR membrane, but it is triggered the same way as I_{CaL} . Due to this mechanism, the model was not able to produce proarrhythmic triggers, such as delayed afterdepolarization (DADs) (Fink et al., 2011).

We reformulated I_{rel} according to the formulation used by Koivumäki et al. (2011) for the human atrial myocyte:

$$I_{\text{rel}} = I_{\text{rel,max}} \cdot \text{RyR}_{\text{CaSR}} \cdot \text{RyR}_o \cdot \text{RyR}_c \cdot (\text{Ca}_{\text{SR}} - \text{Ca}_i)$$

where $I_{\text{rel,max}}$ represents the maximum Ca^{2+} release from SR, RyR_{CaSR} is the dependence on Ca_{SR} , RyR_o is the open (activation) gating variable, RyR_c the closed (inactivation) gating variable. A third gating variable, RyR_a , was used to modulate the working point (adaptation) of the RyR_o and RyR_c gates according to the cytosolic Ca^{2+} concentration as in Koivumäki et al. (2011). The

formulation of the single gating variables is the following

$$\begin{aligned}
 RyR_{CaSR} &= 1 - \frac{1}{1 + e^{\frac{Ca_{SR} - 0.3}{0.1}}} \\
 RyR_{a,ss} &= RyR_{a1} - \frac{RyR_{a2}}{1 + e^{\frac{Ca_i - RyR_{a, half}}{RyR_{a,k}}}} \\
 RyR_{o,ss} &= 1 - \frac{1}{1 + e^{\frac{Ca_i - (RyR_a + RyR_{o, half})}{RyR_{o,k}}}} \\
 RyR_{c,ss} &= \frac{1}{1 + e^{\frac{Ca_i - (RyR_a + RyR_{c, half})}{RyR_{c,k}}}}
 \end{aligned}$$

where the subscript ss indicates the steady state value of the gating variable and the subscripts half and k indicate the half Ca^{2+} concentration and the slope, respectively, of the gating variable steady state. The values of the constants RyR_{a1} , RyR_{a2} and the gating variable half activations $RyR_{a, half}$, $RyR_{o, half}$ and $RyR_{c, half}$ were then optimized (together with other parameters) as described in section “Parameter Optimization.” We report the full set of equations in section 1 of the Supplementary Material.

The formulation of the other SR fluxes, namely the SERCA pump (I_{up}) and the leakage current (I_{leak}) were not changed with respect to the Paci2013 model (Paci et al., 2013). However, their parameters went through the optimization process, as we describe in section Parameter Optimization. In the following we will refer as Paci2013 to the model version presented in Paci et al. (2017).

Parameter Optimization

The parameter optimization process was adapted from Fabbri et al. (2017).

Shortly, parameter optimization was done using the Matlab® function *fminsearch*, which implements the Nelder-Mead Simplex Method, as reported in Fabbri et al. (2017). Such function minimizes a cost function built on the experimental biomarkers we want the model to simulate. The following equations show the cost function structure (Fabbri et al., 2017):

$$\begin{aligned}
 Cost &= \sum_{i=1}^{N_{biomarkers}} Cost_i \\
 Cost_i &= \begin{cases} \frac{|b_{i,Exp} - b_{i,Sim}| - SD_i}{SD_i} \cdot w_i & \text{if } |b_{i,Exp} - b_{i,Sim}| > SD \\ 0 & \text{otherwise} \end{cases}
 \end{aligned}$$

where $Cost_i$ and SD_i represent the cost and the standard deviation for a single biomarker b_i .

The structure of the cost function Cost is consistent with the cost function used in Fabbri et al. (2017). The contribution of each biomarker to the overall cost is zero if the biomarker is within its $\pm SD$ range, otherwise it grows linearly. Moreover, each contribution $Cost_i$ was weighted according to the respective weight w_i . This results in a non-linear cost function, which is zero if all the biomarkers are within the experimental ranges and greater than zero if at least one biomarker is out of range. The AP experimental biomarkers considered for the cost function were:

AP amplitude (APA), maximum diastolic potential (MDP), cycle length (CL), maximum upstroke velocity (V_{max}), AP duration at 10, 30, and 90% of repolarization (APD_{10} , APD_{30} , APD_{90}) and AP shape factor (Triangulation). Triangulation is a shape factor used by Ma et al. (2011) to discriminate between atrial-like ($Triangulation < 1.5$) and ventricular-like ($Triangulation > 1.5$) APs, and it is computed as:

$$Triangulation = \frac{APD_{30} - APD_{40}}{APD_{70} - APD_{80}}$$

The Ca^{2+} transient experimental biomarkers were: duration of the Ca^{2+} transient (DURATION), time to peak (TPEAK), rise time from 10 to 50% (RT_{1050}), rise time from 10 to 90% (RT_{1090}), decay time from 90 to 10% (DT_{9010}) and the Ca^{2+} transient rate (FREQ). The full list of the parameters optimized by this method and their original values are reported in **Table 1**. For optimization, we only chose parameters related to Ca^{2+} handling and additional parameters of I_{NaCa} and the Na^+/K^+ pump (I_{NaK}), i.e., those currents for which the Ma et al. dataset (Ma et al., 2011) did not provide experimental data. The parameter values were constrained in a range $[-20\%, +20\%]$ with respect to their nominal value in the Paci2013 model, in order to avoid non-physiological values, such as negative conductances. The initial parameter values for RyR_{a1} , RyR_{a2} , $RyR_{a, half}$, $RyR_{o, half}$, $RyR_{c, half}$ were rescaled to 1/10 of their values in Koivumäki et al. (2011) before the optimization procedure, in order to adapt them to the Ca^{2+} concentrations in the Paci2013 model, and then optimized as the other parameters. All the other ionic current parameters were kept as in Paci et al. (2013) and Paci et al. (2017) for the late Na^+ current (I_{NaL}) only.

To constrain the model parameters, two different experimental datasets were used. AP data were taken from Ma et al. (2011). This is the same dataset used to calibrate the Paci2013 model and it includes biomarkers computed on spontaneous ventricular-like hiPSC-CM APs recorded at 35–37°C. A second, new, dataset was obtained through Ca^{2+} transient recordings performed at the BioMediTech Institute (Tampere, Finland).

Calcium Recordings in hiPSC-CMs

This study was carried out in accordance with the recommendations of Guidelines of the Ethics Committee of Pirkanmaa Hospital District (Tampere, Finland). The protocol was approved by the Ethics Committee of Pirkanmaa Hospital District (Aalto-Setälä R08070). All subjects gave written informed consent in accordance with the Declaration of Helsinki. New Ca^{2+} transient dataset were recorded at the BioMediTech Institute from healthy control hiPSC-CMs at 35–37°C. The generation and characterization of the control hiPSC line and cardiac differentiation were done as described earlier (Ojala et al., 2016). Cardiomyocytes plated on a coverslip were loaded with 4 μM Fluo-4 AM (Thermo Fisher Scientific) for 30 min and de-esterified for 10 min in perfusate medium: (in mM) 137 NaCl, 5 KCl, 0.44 KH_2PO_4 , 20 HEPES, 4.2 $NaHCO_3$, 5 D-glucose, 2 $CaCl_2$, 1.2 $MgCl_2$, and 1

TABLE 1 | Parameters chosen for optimization.

Parameter	Description	Original value	Optimized value
$V_{\max,up}$ (mM/s)	Maximum Ca^{2+} SERCA uptake	0.56064	0.5113
$I_{rel,max}$ (mM/s)	Maximum Ca^{2+} release current	—	62.5434
RyR_{a1} (μ M)	Adaptation gate constant 1	—	0.05354
RyR_{a2} (μ M)	Adaptation gate constant 2	—	0.0488
$RyR_{a, half}$ (μ M)	Activation gate half Ca^{2+} concentration	—	0.02427
$RyR_{o, half}$ (μ M)	Open gate half Ca^{2+} concentration	—	0.01042
$RyR_{c, half}$ (μ M)	Close gate half Ca^{2+} concentration	—	0.00144
$I_{NaCa,max}$ (pA/pF)	Maximum Na^+/Ca^{2+} exchange current	5.978e3	3917.0463
$I_{NaK,max}$ (pA/pF)	Maximum Na^+/K^+ pump current	2.2958	2.6351
K_{up} (mM)	SERCA half saturation constant	2.5e-4	3.1928e-4
$I_{leak,max}$ (1/s)	Maximum Ca^{2+} leakage flux from SR	4.444e-4	4.7279e-4
alpha (-)	Factor enhancing outward nature of I_{NaCa}	2.8571432	2.5371

For each parameter we reported its original value as in Paci et al. (2017) and the new optimized value. We marked those parameters, which were not included in the old version of the model, as —.

Na-pyruvate dissolved in H_2O (all from Sigma Aldrich). pH of the perfusate medium was adjusted to 7.4 with NaOH (Sigma Aldrich). Perfusate was heated with an inline heater SH-27B controlled with a TC-324B controller unit and input into a RC-25 imaging chamber (all Warner instruments Inc., CT, USA). Calcium kinetics of spontaneously beating cardiomyocytes were imaged with an inverted Olympus IX70 microscope using UApo/340 0,75NA 20x air objective (Olympus, Tokyo, Japan) and recorded with ANDOR iXon 885 EM-CCD camera (Andor Technology, Belfast, Northern Ireland) using 2×2 binning and synchronized with a Polychrome V light source by a real time DPS control unit. LiveAcquisition software (TILL Photonics, Munich, Germany) was used to control light source and camera during recording. Fluo-4 was excited at 490 nm wavelength and the emission was recorded through Olympus U-MF2 Alexa 488 band-pass filter cube (ex.470–495, em.525/50 nm).

Data were recorded from 15 cells for a total of 218 transients. For each biomarker mean value and standard deviation (SD) were computed for model calibration. The experimental values for the biomarkers and their weights are reported in **Table 2**.

Model Validation With Current Blocker Simulations

In order to validate the new hiPSC-CM model after the introduction of the new I_{rel} formulation and the parameters optimization by means of our Ca^{2+} transient data, we chose to

TABLE 2 | Experimental and simulated values of the biomarkers considered for the parameter optimization.

Biomarker	Weight in the cost function	Experimental value (mean \pm SD)	Simulated value
APA (mV)	1	104 \pm 6.0	109.6
MDP (mV)	2	-75.6 \pm 6.6	-75.8
CL (ms)	2	1700.0 \pm 547.7	1549.3
V_{\max} (V/s)	1	27.8 \pm 26.3	24.8
APD ₁₀ (ms)	1	74.1 \pm 26.3	85.8
APD ₃₀ (ms)	1	180 \pm 58.6	241.8
APD ₉₀ (ms)	1	414.7 \pm 119.4	379.8
Triangulation (-)	1	2.5 \pm 1.1	3.0
DURATION (ms)	1	804.5 \pm 188.0	617.8
TPEAK (ms)	1	270.4 \pm 108.3	165.9
RT ₁₀₅₀ (ms)	1	82.9 \pm 50.5	47.7
RT ₁₀₉₀ (ms)	1	167.3 \pm 69.8	106.0
DT ₉₀₁₀ (ms)	1	409.8 \pm 100.1	367.6
FREQ (Hz)	1	0.70 \pm 0.38	0.65

Comparison between the simulated biomarkers and the experimental ones used for the model parameter optimization. AP biomarkers: AP amplitude (APA), maximum diastolic potential (MDP), cycle length (CL), maximum upstroke velocity (V_{\max}), AP duration at 10, 30, and 90% of repolarization (APD₁₀, APD₃₀, APD₉₀) and AP shape factor (Triangulation). Ca^{2+} transient biomarkers: duration of the transient (DURATION), time to peak (TPEAK), rise time from 10 to 50% and to 90% (RT₁₀₅₀, RT₁₀₉₀), decay time from 90 to 10% (DT₉₀₁₀) and the Ca^{2+} transient rate (FREQ).

replicate the current blocker simulations performed in Paci et al. (2013). The model was paced at 1 Hz for 800 s to reach its steady state, then the current blocker was simulated by reducing the maximum conductance of the affected current and finally the AP biomarkers were computed after 400 s. The current blockers considered in the simulations were the same used by Ma et al. (2011): tetrodotoxine (TTX, I_{Na} blocker), nifedipine (NIFED, I_{CaL} blocker), E4031 (I_{Kr} blocker) and 3R4S-Chromanol 293B (CHR, I_{Ks} blocker). For TTX, NIFED and E4031 we considered the following IC_{50} values: 0.64 μ M (Ma et al., 2011), 0.038 μ M (Ma et al., 2011) and 100 nM (Sanguinetti and Jurkiewicz, 1990; Gerlach et al., 2010) respectively. In Ma et al. (2011) CHR had small effects on the AP biomarkers, therefore we tested a range of block levels: 30, 50, 70, and 90%. The stimulus current was 550 pA for NIFED, E4031 and CHR, while we chose 750 pA for TTX in order to trigger APs also at the highest blocker concentrations.

Delayed Afterdepolarizations

In order to trigger DADs in spontaneous APs, Ca^{2+} overload had to be simulated: we chose to increase the superfusate Ca^{2+} concentration (Volders et al., 2000). To ensure that Ca^{2+} overload was simulated only once the model was in steady state, we ran a 800 s simulation without external pacing. From these steady state conditions, we increased the extracellular Ca^{2+} concentration by setting it to 3.945 mM and again we simulated the spontaneous APs. We ran this protocol with both the Paci2013 and the Paci2018 models.

RESULTS

Spontaneous Action Potentials and Ca²⁺ Transients

The automatic optimization process provided a new set of parameters, which is reported in **Table 1**, fourth column. The simulated spontaneous APs and Ca²⁺ transients were in agreement with all the biomarker variability ranges (mean \pm SD), as reported in the last column of **Table 2**. **Figure 1** shows a comparison between the Paci2018 model (in solid blue) and the Paci2013 model (in dashed red). **Figure 2** illustrates the simulated Ca²⁺ transients and traces from four illustrative cells: the comparison highlights that the simulated Ca²⁺ transient contour is fully in agreement with our experiments. In **Figure 3** simulated spontaneous AP and Ca²⁺ traces in steady state are reported, together with the main ionic currents and concentrations. I_{rel} gating variables, together with the Ca²⁺ transients, are detailed in **Figure 4**. It shows that the Ca²⁺ release from SR is not directly dependent on the I_{CaL} activation, but on the cytosolic Ca²⁺ concentration Ca_i , which rules the behavior of the RyR_o, RyR_c, and RyR_a gating variables.

Current Blocker Simulations

We compared in **Table 3** the current blocker effects on the AP biomarkers (i) experimentally recorded by Ma et al. (2011), (ii) simulated by means of the Paci2013 model (Paci et al., 2013), and (iii) simulated by the Paci2018 model. **Figure 5** shows that, despite the changes in the I_{rel} formulation and parameter optimization, the behavior of the Paci2018 model is still consistent with the Paci2013 simulations (Paci et al., 2013) and the experimental data by Ma et al. (2011). TTX affected the upstroke phase, reducing the AP V_{max} and delaying the AP Peak. NIFED, by acting on I_{CaL} , reduced the Ca²⁺ influx through the cell membrane thus reducing the AP duration. Conversely, E4031 reduced the K⁺ efflux through the cell membrane, thus prolonging the AP. Finally, CHR showed little effect on the AP biomarkers, in agreement with the experiments.

Delayed Afterdepolarizations

In **Figure 6** we compared the behavior of the Paci2013 and the Paci2018 models in conditions of high extracellular Ca²⁺ concentration ($Ca_o = 3.945$ mM instead of 1.8 mM) and no external stimulation, i.e., both models produced spontaneous APs. As shown in **Figure 6B**, for $t = [14, 30]$ s I_{rel} underwent a small reactivation, slowing down the decay of the Ca²⁺ transients (**Figure 6E**), affecting the inward component of I_{NaCa} (**Figure 6D**) and triggering DADs in the membrane potential (**Figures 6A,F**). Around $t = 30$ s, I_{rel} underwent a full reactivation, triggering an anticipated Ca²⁺ transient, which resulted in a full anticipated beat (Volders et al., 2000). We reported the extended AP and Ca²⁺ transient traces in the Supplementary Figure 1. Conversely, the old Paci2013 model did not show anomalies in the membrane potential (**Figure 6G**) or Ca²⁺ transients (**Figure 6J**) as consequence of the high extracellular Ca²⁺ concentration, while the Ca²⁺ in SR grew dramatically. The improvements introduced in the Paci2018 model allowed to simulate DADs not only in case of Ca²⁺

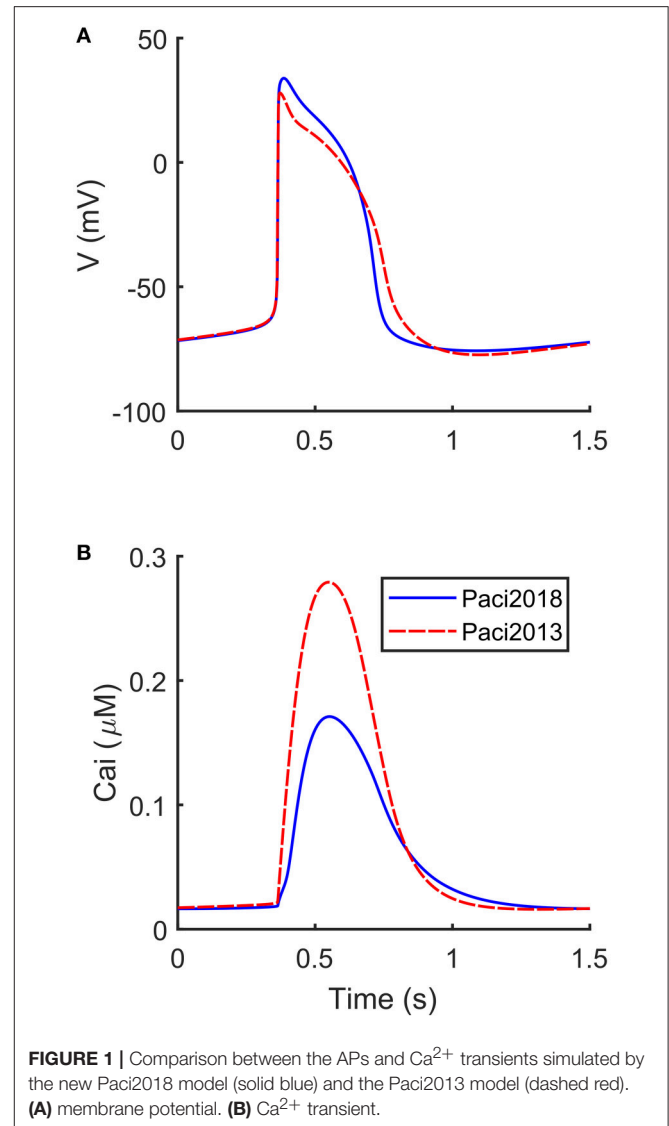


FIGURE 1 | Comparison between the APs and Ca²⁺ transients simulated by the new Paci2018 model (solid blue) and the Paci2013 model (dashed red). **(A)** membrane potential. **(B)** Ca²⁺ transient.

overload, but offered flexibility to simulate behaviors such as the spontaneous premature Ca²⁺ releases reported by Kim et al. (2015) in their Figures 2C, 4B and their Supplemental Figure S1B. We tested also the effect of a rate increment on the generation of DADs in case of hypercalcemia, by providing external pacing. In Supplementary Figure 2, we paced the Paci2018 model at its spontaneous basal rate (38 bpm, in solid blue) and at a basal rate increased by 50% (57 bpm, in dashed red). Despite the shorter diastolic depolarization phase, also at 57 bpm we obtained a fully developed DAD.

Figure 7 shows the spontaneous APs, Ca²⁺ transients and I_{NaCa} , together with the release Ca²⁺ flux (I_{rel}), characterized with premature Ca²⁺ releases. These traces were obtained with a normal extracellular Ca²⁺ concentration ($Ca_o = 1.8$ mM) but simulating more “immature” RyR machinery (namely, by shifting RyR_{o,half} and RyR_{c,half} by -0.002 and 0.002 mM respectively, doubling RyR_o time constant and reducing to half of its nominal value RyR_c time constant). In these conditions of more

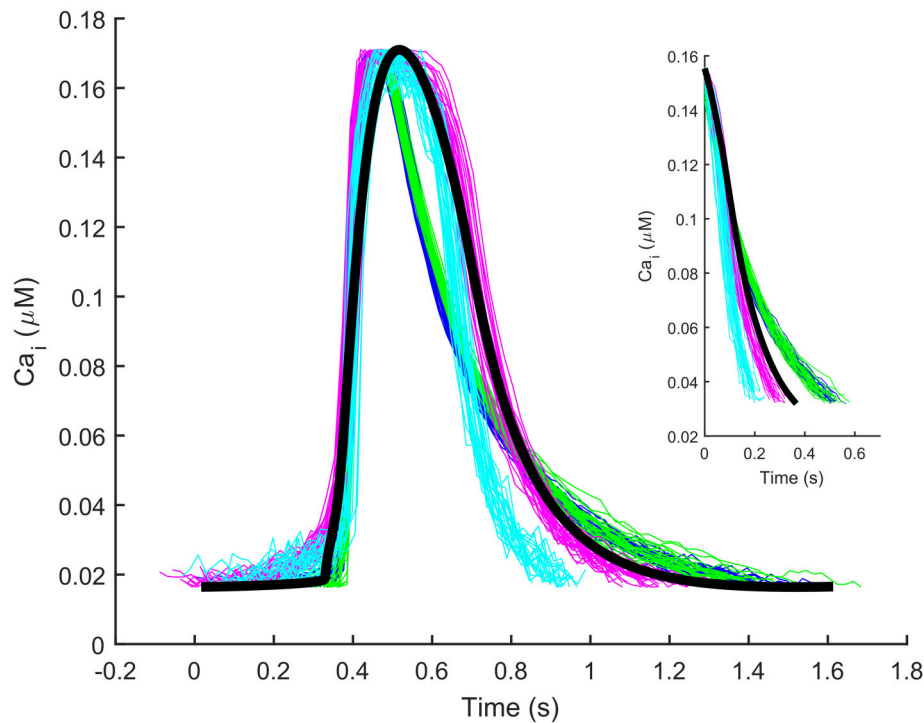


FIGURE 2 | Illustrative experimental Ca^{2+} transients from four cells (blue, cyan, green, magenta) and the Ca^{2+} transient simulated by the Paci2018 model (black). The y-axis of the experimental traces (originally $\Delta F/F$) was normalized between the minimum and maximum values of the simulated trace for comparison. The inset contains only the decay part (from 90 to 10% of the transient amplitude) of the experimental and simulated transients reported in the main Figure.

“immature” RyR machinery, we tested also the effects of I_{NaCa} block on DADs generation. In Supplementary Figure 3, we tested three I_{NaCa} block levels (50, 70, and 90%) while pacing the Paci2018 model at 1 Hz. With no I_{NaCa} block (solid blue trace), APs show small DADs comparable to those reported in Figure 7 in $t = [10, 25]$ s. By blocking 50% of I_{NaCa} (dashed orange trace), we observed that the amplitude of DADs increases. Finally, for the higher block levels, we did not observe any DAD.

Comparison With Other Experimental Data

In order to compare the Paci2018 model with the experimental data, we challenged our model in the following conditions: (i) I_f block by ivabradine, (ii) hyperkalemia, (iii) hypocalcemia.

We simulated I_f block by $3 \mu\text{M}$ ivabradine as a 41% block of I_f maximum conductance (Yaniv et al., 2012; Koivumäki et al., 2018). As shown in Figure 8, I_f block induced only a slight reduction of the frequency of spontaneous APs (-2.3%), in agreement with (Kim et al., 2015), where $3 \mu\text{M}$ had virtually no effects on the spontaneous activity.

Kim et al. (2015) reported a slowdown of the spontaneous activity in conditions of hyperkalemia (from 4 to 8 mM the median frequency dropped from about 1.2 to 0.2 Hz) and a further increase in extracellular K^+ to 12 mM stopped the spontaneous activity. Our single cell model showed a similar trend (although with less sensitivity on K^+): for $\text{K}_o = 8 \text{ mM}$ and $\text{K}_o = 16 \text{ mM}$ the Ca^{2+} transient spontaneous rate dropped by 11% and 15% respectively. An extracellular K^+ concentration

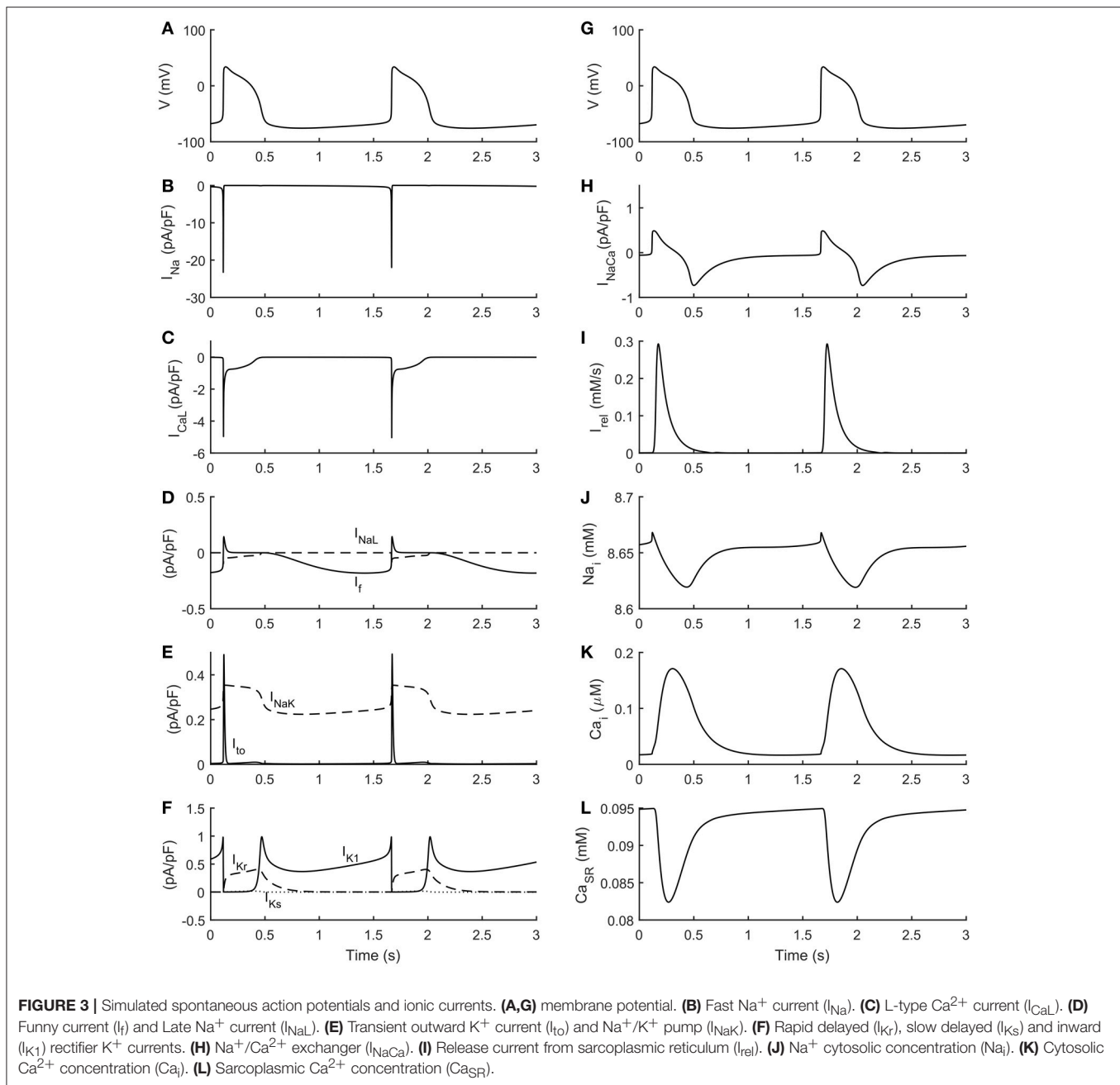
equal to 20 mM stopped the hiPSC-CM spontaneous activity as in Kim et al. (2015).

In the previous section, we tested the model in hypercalcemia conditions to simulate Ca^{2+} overload and the generation of DADs. We also challenged the model with an extracellular Ca^{2+} concentration of 0.1 mM (hypocalcemia) as in Kim et al. (2015): again we observed a trend qualitatively in agreement with the experimental data, since the rate of the spontaneous Ca^{2+} transients dropped by 17%.

DISCUSSION

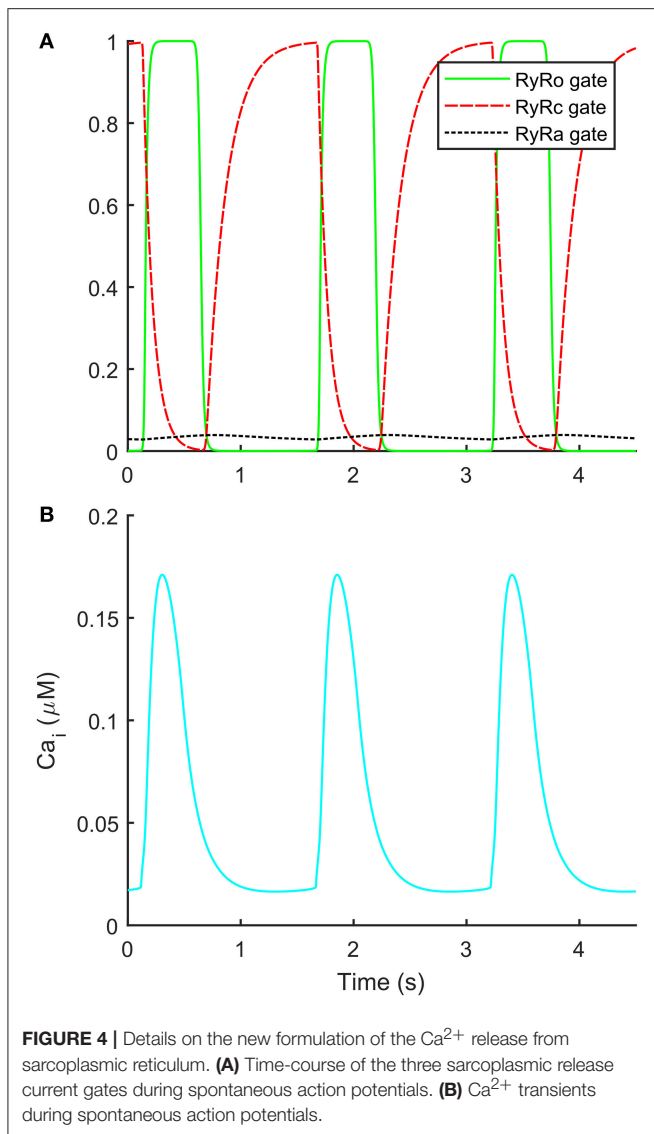
In this paper we present an updated version of the Paci2013 model of ventricular-like hiPSC-CM (Paci et al., 2013), here named Paci2018, developed by exploiting new Ca^{2+} transients data and an automatic algorithm for the parameter optimization.

The Paci2018 model aims to overcome an important limitation of the Paci2013 model, i.e., the simple formulation of the Ca^{2+} release from SR, I_{rel} , initially presented by the TenTusscher2004 model of human adult ventricular cardiomyocyte (ten Tusscher et al., 2004). The peculiarity of such I_{rel} is the direct link between the activation of I_{CaL} and the activation of I_{rel} (through the voltage-dependent activation gating variable d). This I_{rel} formulation was then chosen for its simplicity instead of more complex formulations, however it presumes I_{rel} to be directly dependent on the intracellular



Ca²⁺ concentration and it prevents the model to be able to reproduce Ca²⁺-related anomalies such as DADs. As reported in Fink et al. (2011), models where the open probability of the RyR-sensitive channels is directly dependent on the opening of I_{CaL} are unable to produce DADs. Indeed, DADs start from a repolarized membrane, at potentials where the I_{CaL} gates are closed. Therefore, RyR-sensitive channels have to be able to open even when I_{CaL} is zero, which is not possible in the old I_{rel} formulation. Moreover, the presence of the c_{rel} constant in the TenTusscher2004 I_{rel} formulation could allow a Ca²⁺ flux also from an empty SR, which is clearly not possible.

We chose a quite simple I_{rel} formulation, inspired by the Koivumäki2011 model of human adult atrial cardiomyocyte (Koivumäki et al., 2011), characterized by three gating variables. We did not choose more complex formulations, such as the Markov formulation in TenTusscher2006 model (ten Tusscher and Panfilov, 2006), since the latter was implemented mainly to correctly take into account the presence of T-tubules and the associated microdomains in the human adult ventricular cell. However, hiPSC-CMs produced so far with current differentiation protocols have not shown functional T-tubules (Li et al., 2013).



In order to keep the Paci2018 model the most consistent with its predecessor and with the Ma et al. dataset (Ma et al., 2011) of ionic currents and AP biomarkers, we did not change the formulation of I_{Na} , I_{CaL} , I_{f} , I_{to} , I_{Kr} , I_{Ks} , and I_{K1} , which were carefully fitted for the development of the Paci2013 model. In order to tune the Paci2018 model on the new data of Ca^{2+} transients, we decided to act only on those parameters defining the formulation of currents for which the Ma et al. (2011) dataset did not provide direct experimental data.

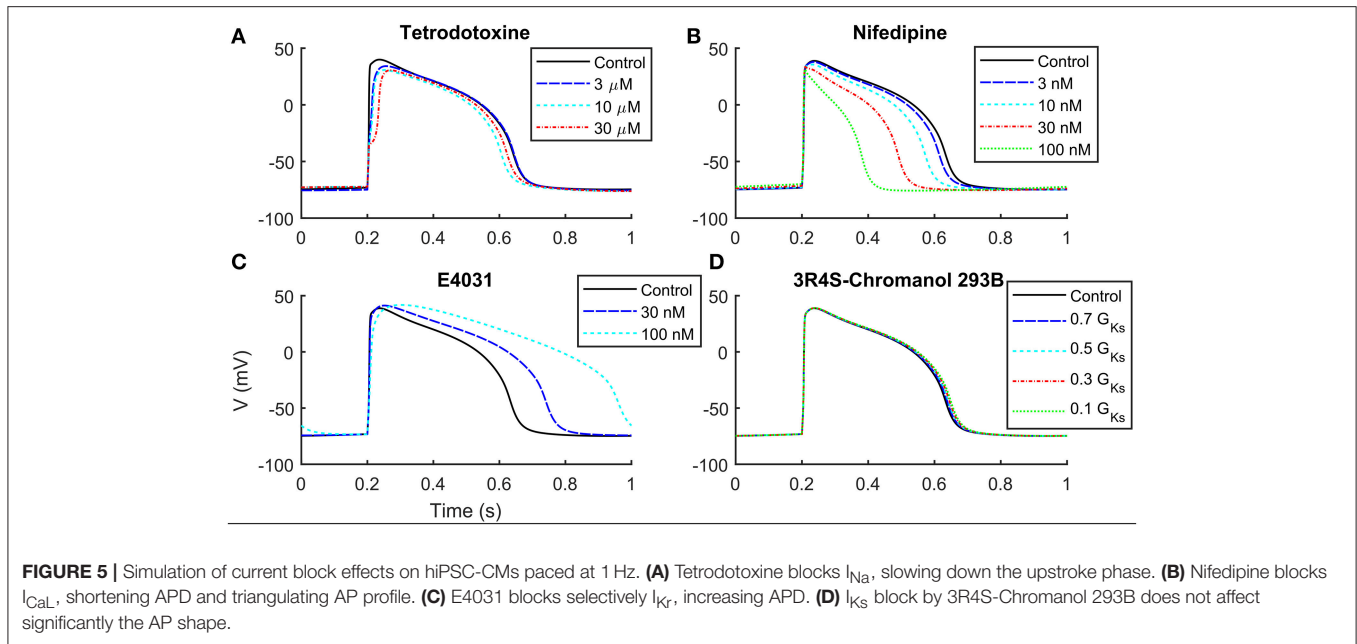
The result is a new model where spontaneous APs match the Ma et al. dataset and where Ca^{2+} transients are in agreement with the new Ca^{2+} dataset. In this paper, we did not aim to propose only modifications to a previous model in order to simulate a specific phenomenon of interest, but we wanted to develop a new cardiac cell model to substantially increase modeling accuracy. Therefore, it was fundamental to check the Paci2018 model capability to reproduce all the experimental data used for the Paci2013 model validation. In detail, we tested the Paci2018

TABLE 3 | Quantitative effects of current blockers on stimulated APs.

AP features	Experiments	Simulations			
		Paci2013		Paci2018	
V_{max}	TTX 3 μM	41.2 \pm 11.2%	18% G_{Na}	26.2%	25.2%
	TTX 10 μM	16.7 \pm 1.8%	6% G_{Na}	23.5%	22.9%
	TTX 30 μM	16.8 \pm 2.0%	2% G_{Na}	20.7%	19.4%
APD ₅₀	E4031 30 nM	109.1 \pm 3.7%	77% G_{Kr}	124.8%	124.9%
	E4031 100 nM	113.4 \pm 3.9%	50% G_{Kr}	160.0%	175.1%
APD ₉₀	E4031 30 nM	140.3 \pm 7.6%	77% G_{Kr}	123.0%	123.4%
	E4031 100 nM	170.4 \pm 13.6%	50% G_{Kr}	151.4%	171.6%
APD ₅₀	Nifed 3 nM	84.6 \pm 2.4%	93% G_{CaL}	94.0%	95.3%
	Nifed 10 nM	70.3 \pm 6.1%	79% G_{CaL}	76.5%	85.2%
	Nifed 30 nM	65.7 \pm 3.0%	56% G_{CaL}	54.9%	65.3%
	Nifed 100 nM	45.4 \pm 4.5%	28% G_{CaL}	33.5%	37.7%
APD ₉₀	Nifed 3 nM	89.4 \pm 1.0%	93% G_{CaL}	96.5%	95.9%
	Nifed 10 nM	78.4 \pm 4.4%	79% G_{CaL}	84.3%	86.2%
	Nifed 30 nM	74.0 \pm 2.3%	56% G_{CaL}	68.8%	67.7%
	Nifed 100 nM	58.2 \pm 5.4%	28% G_{CaL}	51.4%	42.6%

The experimental significant effects ($p < 0.05$) of current blockers on stimulated hiPSC-CMs from Ma et al. (2011) are compared with our previous model (Paci2013) and the current one (Paci2018). Experiments were performed on hiPSC-CMs paced at 1 Hz and are reported in terms of mean \pm SE. Both experimental and simulated values are reported as percent of the control values. For direct comparison, the block levels simulated by the Paci2018 model were computed as in Paci et al. (2013) by means of dose-response curves: TTX ($IC_{50} = 0.64 \mu\text{M}$), Nifed ($IC_{50} = 0.038 \mu\text{M}$) and E4031 ($IC_{50} = 100 \text{ nM}$).

model's responses to the same prototypical current blockers used to validate the Paci2013 model, showing that the behavior of the two models is consistent and in agreement with the experimental data. We further validated the model to simulate the experimentally observed phenomenon of DADs and other specific results obtained in different experimental conditions, being able to replicate all these experiments. In particular, the Paci2018 model can reproduce Ca^{2+} -related abnormalities such as DAD-like anomalies that were not available in old formalism. We observed that the small or full I_{rel} reactivations increase the cytosolic Ca^{2+} concentration and this produces an increased activity of the inward component of I_{NaCa} , which then translates in DAD-like abnormalities in the membrane potential. This is particularly clear in Supplementary Figure 3, where for high levels of I_{NaCa} block (70 and 90%) we do not observe DADs. It is interesting to note that the 50% block is not enough to cancel DADs: in fact, the inward I_{NaCa} component is still strong enough and further enhanced by the cytosolic Ca^{2+} accumulation, due to the very same I_{NaCa} block (minimum diastolic Ca^{2+} : 0.028 vs. 0.017 μM ; average diastolic Ca^{2+} : 0.060 vs. 0.027 μM , in case of 50% I_{NaCa} block or no I_{NaCa} block, respectively). This results in even larger DADs than in the no block case. Similar DAD-like abnormalities in the electrical properties of hiPSC-CMs were also observed in mutant hiPSC lines, such as those derived from patients with HCM (Ojala et al., 2016) or CPVT (Kujala et al., 2012). Of note, in this paper we do not aim to simulate these mutations, which would deserve a specific analysis by their own, but to provide a model which can enable there *in silico* modeling. Notably, the membrane potential and

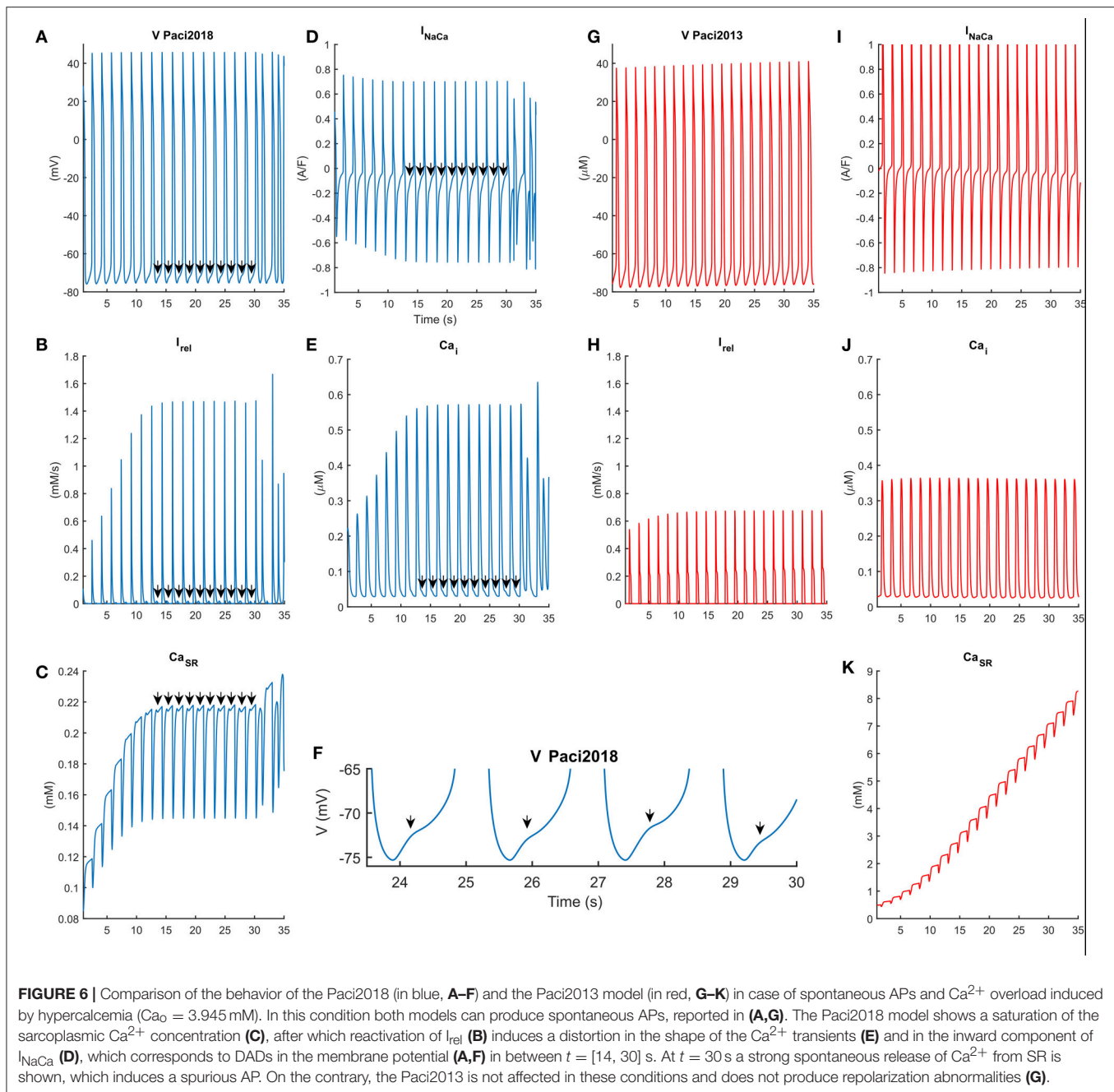


cytosolic Ca^{2+} time-courses obtained by our model are very similar to the experimental ones, as seen by comparison of our **Figures 6, 7** with **Figures 2C, 4B** and **S1** in **Kim et al. (2015)**. In particular, **Figure 4B** in **Kim et al. (2015)** shows the effect of isoproterenol, a non-selective β adrenoceptor agonist, which first induces small delayed spontaneous Ca^{2+} releases and then triggers repetitive high rate firing. In our **Figures 6A,E** we show a very similar pattern in conditions of hypercalcemia (see **Supplementary Figure 1** for an expanded version of Ca^{2+} and AP time-courses), where the spontaneous Ca^{2+} releases, which trigger DADs, finally cause a transition to a higher rate of Ca^{2+} transients and APs.

To further validate our model, we challenged it to simulate specific conditions such as hyperkalemia and hypocalcemia, to compare its behavior to published experimental data. The model showed qualitative agreement with such experiments, in spite of the fact that the spontaneous rate reduction is stronger in the experiments. However, such differences can emerge from (i) the multicellular embryoid body culturing and measurements, i.e., on multicellular ensembles, and especially (ii) as consequence of the high inter-cell line and inter-laboratory variability showed by hiPSC-CMs (**Knollmann, 2013**), especially in beating rate and MDP. In fact, the embryoid bodies examined by **Kim et al. (2015)** exhibited negligible I_{K1} and a much depolarized MDP (-59.1 ± 3.3 mV), which facilitate the spontaneous electrical activity, as shown also by the high frequency of the spontaneous Ca^{2+} transients (1 Hz or higher) in control conditions. On the contrary, the experimental datasets we used in this paper showed slower spontaneous activity and more hyperpolarized MDP, as simulated by our model and reported in **Table 2** (MDP = -75.8 mV, FREQ = 0.65 Hz).

We tested also the capability of the Pac2018 model to simulate early afterdepolarizations (EADs) in conditions of I_{Kr} block: the

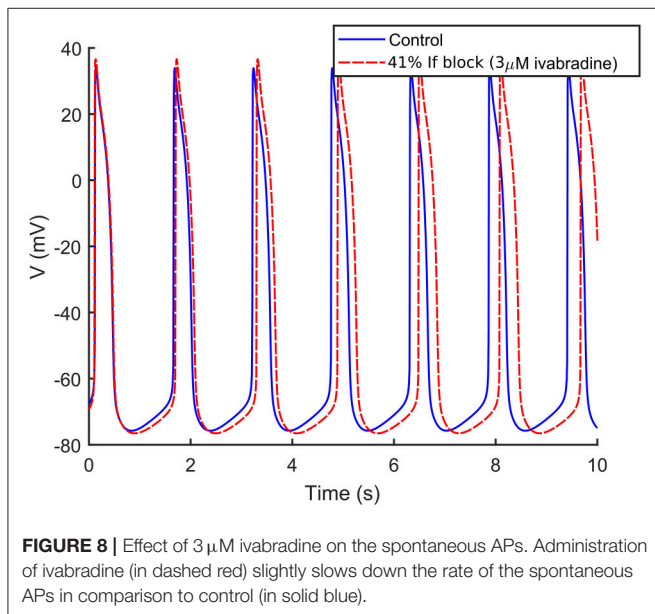
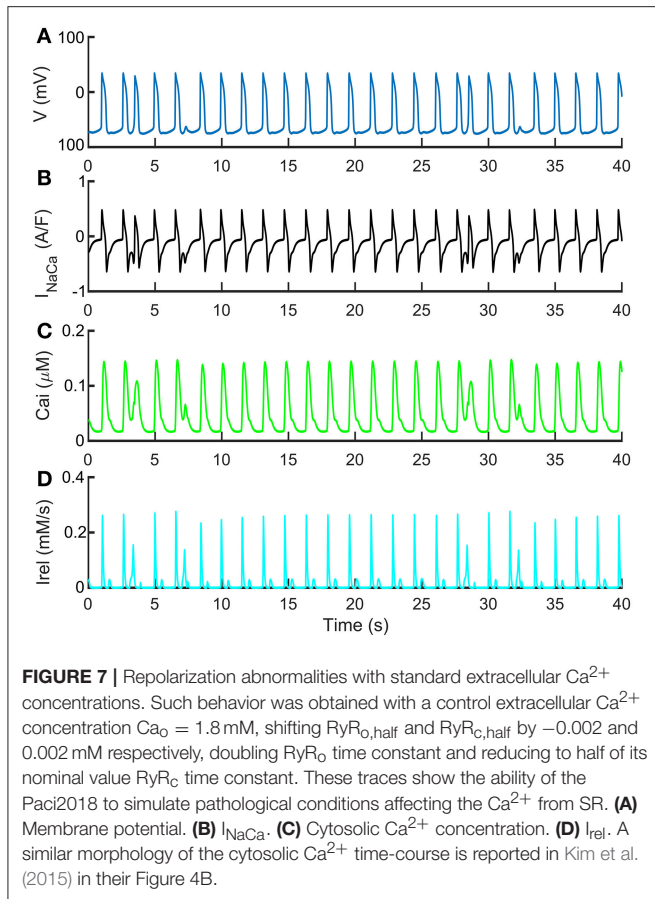
protocol and the results of the EAD simulations were reported in section 3 of the **Supplementary Material**. We observed that the Pac2018, as the old Pac2013 model, does not produce EADs. This is not surprising, since we designed the Pac2018 model carefully maintaining the same formulation for the ion currents that we fit on the experimental data by **Ma et al. (2011)**, and that we used for the Pac2013 model (**Paci et al., 2013**). However, in our previous study (**Paci et al., 2016**), we demonstrated that I_{Kr} block triggered EADs in a population of *in silico* hiPSC-CM based on the Pac2013 model. Replicating here that study is out of the scope of this paper, however we decided to test if two parameter sets, which in **Paci et al. (2016)** triggered EADs, and one parameter set, which triggered repolarization failure, could induce repolarization abnormalities also in the Pac2018 model. **Supplementary Figure 4** shows that, as expected, two derived models produced EADs and the third one repolarization failure. In particular, as reported in the **Supplementary Table 1**, these parameter sets showed (compared to baseline): (i) greater I_{CaL} (which corresponds to a greater Ca^{2+} influx during the repolarization phase in case of I_{CaL} reactivation); (ii) greater I_{NaCa} (which is inward during repolarization, thus promoting abnormalities in conditions of compromised repolarization as in case of I_{Kr} block), and (iii) smaller I_{K1} (corresponding to a smaller contribution to the membrane potential stabilization). It is also interesting to notice that the three parameter sets showed greater I_{Kr} compared to baseline: this suggests that in models where I_{Kr} is highly expressed, a 90% block can have more dramatic effects than in cells expressing smaller I_{Kr} . This small test suggests, as we reported among the limitations, that the use of more refined modeling approaches, e.g., populations of *in silico* models, is advisable to simulate specific phenomena (in this case EADs as consequence of I_{Kr} block) in cell types characterized by high electrophysiological variability. In the perspective of offering



researchers a tool to investigate the mechanisms of ventricular arrhythmia development in hiPSC-CMs, we ran also two preliminary tests about the occurrence of alternans or alternans-like patterns in the Paci2018 model (Methods and Results are detailed in section 4 of the Supplementary Material). When pacing the Paci2018 model at 120 bpm (2 Hz), the membrane potential exhibited an alternans-like pattern, characterized by a full AP followed by a smaller one (Supplementary Figure 5A). We tested also the effect of very high pacing rate (200 bpm, 3.33 Hz) in ischemia-like conditions (Supplementary Figure 5B): in this case, the membrane potential was strongly depolarized

(-60 mV) and exhibited 2:1 alternans. We consider these results valuable also for more advanced studies regarding arrhythmias propagation in case of extension of the simulations to a monodimensional strand or a bidimensional patch.

Overall, we believe that the here presented Paci2018 model substantially increases hiPSC-CM modeling accuracy. Of course, as every *in silico* model, also the Paci2018 is an approximated description of a real system: consequently, new mechanisms can be explored and improved. This is especially true for such a complex cellular system as hiPSC-CM, which is not fully characterized yet. The main limitation that affects the Paci2018



model, as well the other single cell *in silico* models available in literature, is the fact that the simulated behavior belongs to a theoretical cell, built on averaged experimental data from many

cells. In spite of our efforts to build the Paci2018 in a rigorous way, we do not have the presumption to consider it representative of all the hiPSC-CMs available nowadays, both from commercial lines and laboratory-specific lines. This is particularly true in case of an *in vitro* model like hiPSC-CMs, since the same experiments that we need to build an *in silico* model are extremely variable, as reported by multiple studies (Knollmann, 2013; Lu et al., 2015; Paci et al., 2017). As an additional example, in Lu et al. (2015) the authors succeeded in culturing iCell hiPSC-CMs that showed limited biomarker variability. Nevertheless, their cells showed way slower spontaneous beating rate than the cells we used to build our model (~ 15 bpm vs. ~ 38 bpm), despite both datasets were recorded at the same 37°C temperature. In order to have a better translation from *in silico* to *in vitro* models and finally to (pre)clinical applications, more refined modeling techniques exist, e.g., the population of *in silico* models (Britton et al., 2013; Passini et al., 2017). In addition to this, in terms of translation of drug test results from hiPSC-CMs to clinical applications, more challenges emerged recently. For example, in *Abi-Gerges et al. (2017)*, testing a panel of 30 drugs on non-paced hiPSC-CMs provided on one hand good predictivity of pro-arrhythmic events, but on the other hand limited predictivity as an early QT screening. Therefore, in spite the high potential of hiPSC-CMs as *in vitro* models for diseases and drug tests, direct translation of results is still a work in progress, as indicated by the fact that advances in phenotype selection, cell maturation and combined recording platforms are currently being made. One inherent limitation of the Paci2018 model consists in the use of two different datasets of experimental data, one for the AP and ionic current data and the other for Ca^{2+} data. This is clear, e.g., by comparing the mean values of APD_{90} and Ca^{2+} transient DURATION biomarkers: 414.7 and 804.5 ms, respectively. It is known that high affinity Ca^{2+} indicators, such as Fluo-4, can artificially prolong the Ca^{2+} transients and that Ca^{2+} transients last more than APs (Lee et al., 2012); however, the aforementioned Ca^{2+} transient DURATION value is substantially longer than APD_{90} . Therefore, we tried to find an acceptable tradeoff by means of the parameter optimization algorithm, in order to fulfill all the experimental ranges of both the AP and Ca^{2+} transient biomarkers. In particular, in the cost function we chose heavier weights ($w_i = 2$) only for two critical biomarkers which characterize hiPSC-CMs, i.e., MDP (depolarized compared to adult cardiomyocytes) and the rate of the spontaneous APs. For all the other biomarkers, the weights were set to one. The tradeoff obtained by the parameter optimization produced a model that simulates Ca^{2+} transients whose DURATION is 617.8 ms. Despite this value lies within the experimental range 804.5 ± 188.0 ms, it is very close to its lower bound. Conversely, the DT_{9010} biomarker properly lies within its experimental range, although slightly smaller than the experimental mean DT_{9010} (409.8 ± 100.1 vs. 367.6 ms). The inset included in **Figure 2** shows only the decay part (from 90 to 10% of the transient amplitude) of the experimental and simulated transients reported in the main **Figure 2**: our simulated decay lies within the illustrative experimental traces, as well as DT_{9010} of the simulated transient is included in the experimental interval. Of note, the experimental traces reported

in **Figure 2** are purely illustrative of our experiments: the global quantitative comparison between experiments and simulations is done in **Table 2** in terms of biomarkers. It is also known that temperature affects the spontaneous electrical activity of hiPSC-CMs, e.g., in Laurila et al. (2016) the authors showed how the temperature increments and reductions accelerate or slow down hiPSC-CM spontaneous beating, respectively. The fact that the AP and Ca^{2+} transient experimental datasets, chosen to develop the Paci2018 model, were recorded at the same temperature (35–37°C) further mitigates the differences between the two datasets. Another potential limitation of our model is related to its simple structure, consisting of two compartments only (cytosol and SR). Such compartmentalization does not allow to simulate a spatial inhomogeneous Ca^{2+} distribution, as conversely recently done by others (Koivumäki et al., 2018). We preferred to keep the model formulation simple, without entering in such detailed description, since it would have required a more complex mathematical formulation, a more detailed knowledge of the subcellular organization of hiPSC-CMs and, consequently, a more challenging parameter identification and higher simulation time. However, our formulation is successful in simulating the most important electrophysiological mechanisms at the whole cell level, including DADs elicited from different kind of stresses, without resorting to random RyR openings, as done in Koivumäki et al. (2018). A final limitation of the Paci2018 model is that it describes only the electrophysiology and the Ca^{2+} handling, but it does not take into consideration contractility. In literature, a few models of myofilament are available (Negroni and Lascano, 2008; Rice et al., 2008; Negroni et al., 2015). For instance, in Negroni et al. (2015) the authors presented an integrated rabbit ventricular cardiomyocyte model, which included also the mathematical description of force generation and the myofilament Ca^{2+} kinetics. However, the sarcomeric structure of hiPSC-CMs is immature and the myofibrils in hiPSC-CMs are oriented in multiple directions within the cell: in Bedada et al. (2016) a higher level of sarcomeric organization was reached only by repopulating hiPSC-CMs into a biological cardiac matrix. We acknowledge the potential of an integration of the myofilament description in the Paci2018, nevertheless the translation from a different species model of, e.g., rabbit cardiomyocyte to a hiPSC-CM model is not elementary and out of the scope of this paper. Future developments of this work will include using the Paci2018 model to ran *in silico* drug tests and to

ran monodimensional and bidimensional simulations, as done, e.g., by Raphel et al. with the Paci2013 model (Raphel et al., 2017).

In conclusion, in this work we present an updated and more versatile version of our hiPSC-CM *in silico* model, based on a new dataset of electrophysiological data. Our model can represent the basis for new *in silico* studies on the effects of drugs or mutations (e.g., CPVT), which affect the Ca^{2+} handling in hiPSC-CMs. Due to its relatively light formulation (23 ordinary differential equations), our model is suitable also for very large studies on *in silico* populations, e.g., to support screening of different drug/compounds at various concentrations.

AUTHOR CONTRIBUTIONS

All the authors conceived and designed the study. R-PP and KP performed the *in vitro* measurements and analyzed the *in vitro* data. MP and DC performed the *in silico* model development and validation. MP and SS analyzed the *in silico* data, prepared the figures and drafted the manuscript. All the authors interpreted the results and revised the manuscript.

FUNDING

MP was financially supported by the Academy of Finland (project CardSiPop, decision number 307967). R-PP was financially supported by Paavo Nurmi Foundation. The Heart Group has been supported by the Finnish Cardiovascular Foundation, the Academy of Finland, TEKES—the Finnish Funding Agency for Innovation and Technology, and Pirkanmaa Hospital District.

ACKNOWLEDGMENTS

The authors acknowledge CSC—IT Center for Science, Finland, for generous computational resources, Tampere Facility of Electrophysiological Measurements for their service and Dr. Jussi Koivumäki for sharing his code.

SUPPLEMENTARY MATERIAL

The Supplementary Material for this article can be found online at: <https://www.frontiersin.org/articles/10.3389/fphys.2018.00709/full#supplementary-material>

REFERENCES

- Abi-Gerges, N., Pointon, A., Oldman, K. L., Brown, M. R., Pilling, M. A., Sefton, C. E., et al. (2017). Assessment of extracellular field potential and Ca^{2+} transient signals for early QT/pro-arrhythmia detection using human induced pluripotent stem cell-derived cardiomyocytes. *J. Pharmacol. Toxicol. Methods* 83, 1–15. doi: 10.1016/j.vascn.2016.09.001
- Ahola, A., Pölonen, R. P., Aalto-Setälä, K., and Hyttinen, J. (2018). Simultaneous measurement of contraction and calcium transients in stem cell derived cardiomyocytes. *Ann. Biomed. Eng.* 46, 148–158. doi: 10.1007/s10439-017-1933-2
- Bedada, F. B., Wheelwright, M., and Metzger, J. M. (2016). Maturation status of sarcomere structure and function in human iPSC-derived cardiac myocytes. *Biochim. Biophys. Acta* 1863, 1829–1838. doi: 10.1016/j.bbamcr.2015.11.005
- Björk, S., Ojala, E. A., Nordström, T., Ahola, A., Liljeström, M., Hyttinen, J., et al. (2017). Evaluation of optogenetic electrophysiology tools in human stem cell-derived cardiomyocytes. *Front. Physiol.* 8:884. doi: 10.3389/fphys.2017.00884
- Britton, O. J., Bueno-Orovio, A., Van Ammel, K., Lu, H. R., Towart, R., Gallacher, D. J., et al. (2013). Experimentally calibrated population of models predicts and explains intersubject variability in cardiac cellular electrophysiology. *Proc. Nat. Aca. Sci. U.S.A.* 110, E2098–E2105. doi: 10.1073/pnas.1304382110

- Entcheva, E., and Bub, G. (2016). All-optical control of cardiac excitation: combined high-resolution optogenetic actuation and optical mapping. *J. Physiol.* 9, 2503–2510. doi: 10.1113/JP271559
- Fabbri, A., Fantini, M., Wilders, R., and Severi, S. (2017). Computational analysis of the human sinus node action potential: model development and effects of mutations. *J. Physiol.* 7, 2365–2396. doi: 10.1113/JP273259
- Fink, M., Noble, P. J., Noble, D., Fink, M., Noble, P. J., and Noble, D. (2011). Ca²⁺-induced delayed afterdepolarizations are triggered by dyadic subspace Ca⁺ affirming that increasing SERCA reduces aftercontractions. *Cardiac Excit. Contract.* 301, 921–935. doi: 10.1152/ajpheart.01055.2010
- Gerlach, A. C., Stoehr, S. J., and Castle, N. A. (2010). pharmacological removal of human ether-à-go-related gene potassium channel inactivation by 3-nitro-N-(4-phenoxyphenyl) benzamide (ICA-105574). *Mol. Pharmacol.* 77, 58–68. doi: 10.1124/mol.109.059543
- Kim, J. J., Yang, L., Lin, B., Zhu, X., Sun, B., Kaplan, A. D., et al. (2015). Mechanism of automaticity in cardiomyocytes derived from human induced pluripotent stem cells. *J. Mol. Cell. Cardiol.* 81, 81–93. doi: 10.1016/j.yjmcc.2015.01.013
- Klimas, A., Ambrosi, C. M., Yu, J., Williams, J. C., Bien, H., and Entcheva, E. (2016). OptoDyCE as an automated system for high-throughput all-optical dynamic cardiac electrophysiology. *Nat. Commun.* 7:11542. doi: 10.1038/ncomms11542
- Knollmann, B. C. (2013). Induced pluripotent stem cell-derived cardiomyocytes: boutique science or valuable arrhythmia model? *Circ. Res.* 112, 969–976. doi: 10.1161/CIRCRESAHA.112.300567
- Koivumäki, J. T., Korhonen, T., and Tavi, P. (2011). Impact of sarcoplasmic reticulum calcium release on calcium dynamics and action potential morphology in human atrial myocytes: a computational study. *PLoS Comput. Biol.* 7:e1001067. doi: 10.1371/journal.pcbi.1001067
- Koivumäki, J. T., Naumenko, N., Tuomainen, T., Takalo, J., Oksanen, M., Puttonen, K. A., et al. (2018). Structural immaturity of human iPSC-derived cardiomyocytes: *in silico* investigation of effects on function and disease modeling. *Front. Physiol.* 9:80. doi: 10.3389/fphys.2018.00080
- Kujala, K., Paavola, J., Lahti, A., Larsson, K., Pekkanen-Mattila, M., Viitasalo, M., et al. (2012). Cell model of catecholaminergic polymorphic ventricular tachycardia reveals early and delayed afterdepolarizations. *PLoS ONE* 7:e44660. doi: 10.1371/journal.pone.0044660
- Lahti, A. L., Kujala, V. J., Chapman, H., Koivisto, A.-P., Pekkanen-Mattila, M., Kerkela, E., et al. (2012). Model for long QT syndrome type 2 using human iPSC cells demonstrates arrhythmogenic characteristics in cell culture. *Dis. Model. Mech.* 220–230. doi: 10.1242/dmm.008409
- Laurila, E., Ahola, A., Hyttinen, J., and Aalto-Setälä, K. (2016). Methods for *in vitro* functional analysis of ipsc derived cardiomyocytes—special focus on analyzing the mechanical beating behavior. *Biochim. Biophys. Acta* 1863, 1864–1872. doi: 10.1016/j.bbamer.2015.12.013
- Lee, P., Klos, M., Bollensdorff, C., Hou, L., Ewart, P., Kamp, T. J., et al. (2012). Simultaneous voltage and calcium mapping of genetically purified human induced pluripotent stem cell-derived cardiac myocyte monolayers. *Circ. Res.* 110, 1556–1563. doi: 10.1161/CIRCRESAHA.111.262535
- Lei, C. L., Wang, K., Clerx, M., Johnstone, R. H., Hortigon-Vinagre, M. P., Zamora, V., et al. (2017). Tailoring mathematical models to stem-cell derived cardiomyocyte lines can improve predictions of drug-induced changes to their electrophysiology. *Front. Physiol.* 8:986. doi: 10.3389/fphys.2017.00986
- Li, S., Chen, G., and Li, R. A. (2013). Calcium signalling of human pluripotent stem cell-derived cardiomyocytes. *J. Physiol.* 591, 5279–5290. doi: 10.1113/jphysiol.2013.256495
- Lu, H. R., Whittaker, R., Price, J. H., Vega, R., Pfeiffer, E. R., Cerignoli, F., et al. (2015). High throughput measurement of Ca⁺⁺ dynamics in human stem cell-derived cardiomyocytes by kinetic image cytometry: a cardiac risk assessment characterization using a large panel of cardioactive and inactive compounds. *Toxicol. Sci.* 148, 503–516. doi: 10.1093/toxsci/kfv201
- Ma, D., Wei, H., Zhao, Y., Lu, J., Li, G., Binte, N., et al. (2013). Modeling type 3 Long QT syndrome with cardiomyocytes derived from patient-specific induced pluripotent stem cells. *Int. J. Cardiol.* 168, 5277–5286. doi: 10.1016/j.ijcard.2013.08.015
- Ma, J., Guo, L., Fiene, S. J., Anson, B. D., Thomson, J. A., Kamp, T. J., et al. (2011). High purity human-induced pluripotent stem cell-derived cardiomyocytes: electrophysiological properties of action potentials and ionic currents. *Am. J. Physiol. Heart Circ. Physiol.* 301, H2006–H2017. doi: 10.1152/ajpheart.00694.2011
- Moretti, A., Bellin, M., Welling, A., Jung, C. B., Lam, J. T., Bott-Flügel, L., et al. (2010). Patient-specific induced pluripotent stem-cell models for long-qt syndrome. *N. Engl. J. Med.* 363, 1397–1409. doi: 10.1056/NEJMoa0908679
- Negroni, J. A., and Lascano, E. C. (2008). Simulation of steady state and transient cardiac muscle response experiments with a huxley-based contraction model. *J. Mol. Cell. Cardiol.* 45, 300–312. doi: 10.1016/j.yjmcc.2008.04.012
- Negroni, J. A., Morotti, S., Lascano, E. C., Gomes, A. V., Grandi, E., Puglisi, J. L., et al. (2015). β -Adrenergic effects on cardiac myofilaments and contraction in an integrated rabbit ventricular myocyte model. *J. Mol. Cell. Cardiol.* 81, 162–175. doi: 10.1016/j.yjmcc.2015.02.014
- Ojala, M., Prajapati, C., Pekka Pölonen, R., Rajala, K., Pekkanen-Mattila, M., Rasku, J., et al. (2016). Mutation-Specific Phenotypes in hiPSC-Derived Cardiomyocytes Carrying Either Myosin-Binding Protein C or α -Tropomyosin Mutation for Hypertrophic Cardiomyopathy. *Stem Cell Int.* 2016:1684792. doi: 10.1155/2016/1684792
- Paci, M., Hyttinen, J., Aalto-Setälä, K., and Severi, S. (2013). Computational models of ventricular- and atrial-like human induced pluripotent stem cell derived cardiomyocytes. *Ann. Biomed. Eng.* 41, 2334–2348. doi: 10.1007/s10439-013-0833-3
- Paci, M., Hyttinen, J., Rodriguez, B., and Severi, S. (2015). Human induced pluripotent stem cell-derived versus adult cardiomyocytes: an *in silico* electrophysiological study on effects of ionic current block. *Br. J. Pharmacol.* 172, 5147–5160. doi: 10.1111/bph.13282
- Paci, M., Passini, E., Severi, S., Hyttinen, J., and Rodriguez, B. (2016). A population of *in silico* models to face the variability of human induced pluripotent stem cell-derived cardiomyocytes: the hERG block case study. *Comput. Cardiol.* 43, 1189–1192. doi: 10.23919/CIC.2016.7868961
- Paci, M., Passini, E., Severi, S., Hyttinen, J., and Rodriguez, B. (2017). Phenotypic Variability in LQT3 Human induced pluripotent stem cell-derived cardiomyocytes and their response to antiarrhythmic pharmacologic therapy: an *in silico* approach. *Heart Rhythm* 14, 1704–1712. doi: 10.1016/j.hrthm.2017.07.026
- Paci, M., Sartiani, L., Lungo, M., Jaconi, M., Mugelli, A., Cerbai, E., et al. (2012). Mathematical modelling of the action potential of human embryonic stem cell derived cardiomyocytes. *Biomed. Eng. Online* 11:61. doi: 10.1186/1475-925X-11-61
- Passini, E., Britton, O. J., Lu, H. R., Rohrbacher, J., Hermans, A. N., Gallacher, D. J., et al. (2017). Human *in silico* drug trials demonstrate higher accuracy than animal models in predicting clinical pro-arrhythmic cardiotoxicity. *Front. Physiol.* 8:668. doi: 10.3389/fphys.2017.00668
- Rajamohan, D., Kalra, S., Hoang, M. D., George, V., Staniforth, A., Russell, H., et al. (2016). Automated electrophysiological and pharmacological evaluation of human pluripotent stem cell-derived cardiomyocytes. *Stem Cells Dev.* 25, 439–452. doi: 10.1089/scd.2015.0253
- Raphel, F., Boulakia, M., Zenzemi, N., Coudiere, Y., Guillon, J.-M., Zitoun, P., et al. (2017). identification of ion currents components generating field potential recorded in MEA from hiPSC-CM. *IEEE Trans. Biomed. Eng.* 9294, 1–1. doi: 10.1109/TBME.2017.2748798
- Rice, J. J., Wang, F., Bers, D. M., and De Tombe, P. P. (2008). Approximate model of cooperative activation and crossbridge cycling in cardiac muscle using ordinary differential equations. *Biophys. J.* 95, 2368–2390. doi: 10.1529/biophysj.107.119487
- Sanguinetti, M. C., and Jurkiewicz, N. K. (1990). Two Components of cardiac delayed rectifier K⁺ current. differential sensitivity to block by class III antiarrhythmic agents. *J. Gen. Physiol.* 96, 195–215. doi: 10.1085/jgp.96.1.195
- Takahashi, K., Tanabe, K., Ohnuki, M., Narita, M., Ichisaka, T., Tomoda, K., et al. (2007). Induction of pluripotent stem cells from adult human fibroblasts by defined factors. *Cell* 131, 861–872. doi: 10.1016/j.cell.2007.11.019
- ten Tusscher, K. H. W. J., Noble, D., Noble, P. J., and Panfilov, A. V. (2004). A model for human ventricular tissue. *Am. J. Physiol. Heart Circ. Physiol.* 286, H1573–H1589. doi: 10.1152/ajpheart.00794.2003
- ten Tusscher, K. H., and Panfilov, A. V. (2006). Alternans and spiral breakup in a human ventricular tissue model. *Am. J. Physiol. Heart Circ. Physiol.* 291, H1088–H1100. doi: 10.1152/ajpheart.00109.2006

- Volders, P. G., Vos, M. A., Szabo, B., Sipido, K. R., de Groot, S. H., Gorgels, A. P., et al. (2000). progress in the understanding of cardiac early afterdepolarizations and torsades de pointes: time to revise current concepts. *Cardiovas. Res.* 46, 376–92. doi: 10.1016/S0008-6363(00)0022-5
- Walker, C. A., and Spinale, F. G. (1999). The structure and function of the cardiac myocyte: a review of fundamental concepts. *J. Thorac. Cardiovasc. Surg.* 118, 375–382. doi: 10.1016/S0022-5223(99)70233-3
- Yaniv, Y., Maltsev, V. A., Ziman, B. D., Spurgeon, H. A., and Lakatta, E. G. (2012). The ‘funny’ current (If) inhibition by ivabradine at membrane potentials encompassing spontaneous depolarization in pacemaker cells. *Molecules* 17, 8241–8254. doi: 10.3390/molecules17078241

Conflict of Interest Statement: The authors declare that the research was conducted in the absence of any commercial or financial relationships that could be construed as a potential conflict of interest.

The reviewer JB and handling Editor declared their shared affiliation.

Copyright © 2018 Paci, Pölonen, Cori, Penttinen, Aalto-Setälä, Severi and Hyttinen. This is an open-access article distributed under the terms of the Creative Commons Attribution License (CC BY). The use, distribution or reproduction in other forums is permitted, provided the original author(s) and the copyright owner are credited and that the original publication in this journal is cited, in accordance with accepted academic practice. No use, distribution or reproduction is permitted which does not comply with these terms.